

Bose-Einstein Condensate Dark Matter Halos confronted with galactic observations

M. Dworknik^{1,2}, Z. Keresztes^{1,2} and L. Á. Gergely^{1,2,3}

¹Department of Theoretical Physics, University of Szeged,
Kossuth Lajos sgt. 42, Szeged 6724, Hungary

²Department of Experimental Physics, University of
Szeged, Dóm Tér 9, Szeged 6720, Hungary

³Department of Physics, Faculty of Science, Tokyo
University of Science, 1-3, Shinjuku-ku, Tokyo 162-8601,
Japan

Abstract. We present a comparative confrontation of both the Bose-Einstein Condensate (BEC) and the Navarro-Frenk-White (NFW) dark halo models with galactic rotation curves and velocity dispersion data. We conclude that the BEC model fits better the dwarf galaxy dark matter distribution, but suffers from sharp cut-off in larger galaxies, where the NFW model performs better. In more detail, we employ 6 High Surface Brightness (HSB), 6 Low Surface Brightness (LSB) and 7 dwarf galaxies with rotation curves falling into two classes, based on their shapes. In the first class the rotational velocities increase with radius over the whole observed range, the BEC and NFW models giving comparable fits for both HSB and LSB galaxies, while significantly improving over the NFW fit for dwarf galaxies. This improvement is due to the central density cusp avoidance property of the BEC model. The rotational velocity of HSB and LSB galaxies falling into the second class exhibit long flat plateaus, resulting in a better fit of the NFW model for HSB galaxies, and comparable fits for LSB galaxies. The weaker performance of the BEC model for the HSB type II galaxies is due to the BEC density profiles dropping rapidly to zero outside a nearly constant density core. Finally we confront both models with the projected velocity dispersion profiles of 6 Virgo cluster galaxies, which after a steep rising, remain flat over the sampled region. The two models gave comparable combined χ^2_{\min} values for these galaxies but both model fits remained outside the 3σ confidence level, pointing out the need for a better modelling of the velocity dispersion of galaxies that both the BEC and NFW models could provide.

1. Introduction

The visible part of most galaxies is embedded in a dark matter (DM) halo of yet unknown composition, observable only through its gravitational interaction with the baryonic matter. Assuming the standard Λ CDM cosmological model, the Planck satellite measurements of the cosmic microwave background anisotropy power spectrum support 4.9% baryonic matter, 26.8% DM and 68.3% dark energy in the Universe [1]; [2].

The mass distribution of spiral galaxies is essential for investigating DM. Beside the stellar disk and central bulge, most of the galaxies harbour a spherically symmetric, massive DM halo, which dominates the dynamics in the stellar disk at the outer

regions. Nevertheless there are examples of galaxies which at larger radii are better described by a flattened baryonic mass distribution (global disk model) [3].

Several DM candidates and alternatives have been proposed, the latter assuming Einstein's theory of gravity breaking down on the galactic scale and above ([4]; [5]; [6]; [7]; [8]; [9]; [10]; [11]; [12]). In brane-world and f(R)-gravity models, the galactic rotation curves could be explained without DM ([13]; [14]; [15]; [16]).

It is well known that hot dark matter (HDM) consisting of light ($m \propto \text{eV}$) particles cannot reproduce the cosmological structure formation, as they imply that the superclusters of galaxies are the first structures to form contradicting CMB observations, according to which superclusters would form at the present epoch [17]. Warm dark matter ($m \propto \text{keV}$) models seem to be compatible with the astronomical observations on galactic and also cosmological scales [18]; [19]. Leading candidates for warm dark matter are the right handed neutrinos, which in contrast with their left handed counterparts do not participate in the weak interaction. The decay of these sterile neutrinos produces high amount of X-rays, which can boost the star formation rate leading to an earlier reionization [20]. Cold dark matter (CDM) also shows remarkably good agreement with observations over kpc scales ([21]; [22]). Particular CDM candidates, like neutralinos (which is stable and can be produced thermally in the early Universe) and other weakly interacting massive particles (WIMPs) originating in supersymmetric extensions of the Standard Model were severely constrained by recent LHC results, rendering them into the range $200\text{GeV} \lesssim m_n \lesssim 500\text{GeV}$ [23]. In a Higgs-portal DM scenario the Higgs boson acts as the mediator particle between DM and Standard Model particles, and it can decay to a pair of DM particles. Very recent constraints established by the ATLAS Collaboration on DM-nucleon scattering cross section impose upper limits of approximately 60 GeV for each of the scalar, fermion and vector DM candidates (see Fig. 4 of Ref. [24]), within the framework of this scenario.

Large N-body simulations (e.g. [25]) performed in the framework of the Λ CDM-model (Λ being the cosmological constant) predict that CDM halos surrounding galaxies must have central density cusps [26]. The cusps appear in the Navarro-Frenk-White (NFW) DM density profile $\rho_{NFW}(r) = \rho_s/(r/r_s)(1+r/r_s)^2$, where r_s is a scale radius and ρ_s is a characteristic density. On the observational side however, high-resolution rotation curves show instead that the distribution of DM in the centres of DM dominated dwarf and Low Surface Brightness (LSB) galaxies is much shallower, exhibiting a core with nearly constant density [27]. On the other hand the NFW model is remarkably successful on Mpc scales. The surface number-density profiles of satellites decline with the projected distance as a power law with the slope $-2 \div -1.5$, while the line-of-sight velocity dispersions decline gradually [28]. These observations support the NFW model on scales of 50-500 kpc.

In a cosmological treatment various scalar field dark matter models are also successfully employed see Ref. [29] and references therein. A particular scalar field DM model describes light bosons in a dilute gas. The thermal de Broglie wavelength of the particles is $\lambda_T \propto 1/\sqrt{mT}$, which can be large for light bosons ($m < \text{eV}$) and for low temperature. Below a critical temperature (T_c), the bosons' wave packets, which are the order of λ_T -overlap, resulting in correlated particles. Such bosons share the same quantum ground state, behaving as a Bose-Einstein condensate (BEC), characterized by a single macroscopic wave function. It has been proposed that galactic DM halos could be gigantic BECs [30]. The self gravitating condensate is described by the Gross-Pitaevskii-Poisson equation system in the mean-field approximation [31], [32],

[33], [10]. In the Thomas-Fermi approximation, a 2-parameter (mass m and scattering length a) density distribution of the BEC halo is obtained [see Eq. (3) below] which is less concentrated towards the centre as compared to the NFW model, relaxing the cuspy halo problem.

In Ref. [34] the authors study a model where a normal dark matter phase with an equation of state $P = \rho c^2 \sigma_{tr}^2$ condensed into a BEC. Here σ_{tr} is the one-dimensional velocity dispersion and c is the speed of light. Requiring the continuity of the pressure at the transition point, the condensation occurs at a redshift $1 + z_c \approx 1.22 \times 10^3 (m/10^{-33}g)^{1+\sigma_{tr}^2} (\sigma_{tr}^2/3 \times 10^{-6})^{1/3(1+\sigma_{tr}^2)} (a/10^{-10}cm)^{-1/3(1+\sigma_{tr}^2)}$ with a critical temperature of $T_c \approx 6.57 \times 10^3 (m/10^{-33}g)^{1/3} (\sigma_{tr}^2/3 \times 10^{-6})^{2/3} (a/10^{-10}cm)^{-2/3}$ K. The values of the parameters m , a and σ_{tr} are quite uncertain for dark matter particles. Adopting the numerical value $\sigma_{tr} = 0.0017$ [34] and assuming $z_c > 900$, then taking the scattering lengths: $a = 10^3$ fm, $a = 10^{-14}$ fm and $a = 10^{-55}$ fm we find the following mass ranges: $m > 1$ eV, $m > 2 \times 10^{-6}$ eV and $m > 4.57 \times 10^{-20}$ eV, respectively. The stability of the BEC halo depends on the particle mass and scattering length. For a given mass the stability occurs for larger scattering length and for given scattering length the stability appears at smaller mass. Galactic size stable halos can form with $m > 10^{-24}$ eV (see Fig. 3. in Ref. [35]). For the masses and scattering lengths considered above the halos are stable and they fall into the galactic size range.

A recent investigation shows that a stable BEC halo can be formed as a result of gravitational collapse [36]. The model has been tested on kpc scales confronting it with galactic rotation curve observations [10]. The BEC model can explain the observed collisional behaviour of DM in the Abell 520 cluster [37] and the acoustic peaks of the cosmic microwave background (BEC could mimic the effects of the standard CDM in the CMB spectrum) [38]. It was pointed out by [39] that the effects of BEC DM should be seen in the matter power spectrum if the boson mass is in the range $15 \text{ meV} < m < 35 \text{ meV}$ and $300 \text{ meV} < m < 700 \text{ meV}$ for the scattering lengths $a = 10^6$ fm and $a = 10^{10}$ fm, respectively. All of the mentioned BEC particle masses are consistent with the limit $m < 1.87$ eV imposed from galaxy observations and N-body simulation [40].

A discrepancy was pointed out between the best fit density profile parameters derived from the strong lensing and the galactic rotational curves data [41]. However the lensing and rotational curve tests employed different galaxy samples.

In this work we propose to critically examine the BEC model against rotation curve and velocity dispersion data, investigating BEC as a possible DM candidate and pointing out both advantages and disadvantages over the NFW model. Previous studies on the compatibility of the BEC model and galactic rotation curves were promising, but relied on a less numerous and less diversified set of galaxies then employed here ([42], [43]). The paper is organized as follows. The basic properties of the BEC DM model are reviewed in Section 2. In Section 3 the theoretical predictions of the BEC model are compared with the observed rotation curve data of three types of galaxies, the High Surface Brightness (HSB), LSB and dwarf galaxies. Measurement of the stellar velocity dispersion provides an additional method to determine the density distribution in galaxies. The Virgo Cluster, as the nearest and one of the most extensively studied galaxy clusters due to its relative proximity (16.5 Mpc) offers thousands of well-resolved galaxies. In Section 4 we present the results of a combined test with velocity dispersion profiles and rotation curves of 6 Virgo cluster galaxies and derive the best fit parameters of the BEC and NFW dark matter models. The conclusions are presented in Section 5.

2. The Bose-Einstein condensate galactic dark matter halo

An ideal, dilute Bose gas at very low temperature forms a Bose-Einstein condensate in which all particles are in the same ground state. In the thermodynamic limit, the critical temperature for the condensation is $T_c = 2\pi\hbar^2 (n/\zeta)^{3/2} / mk_B$ [44]. Here n and m are the number density and the mass of the bosons, respectively, $\zeta = 2.612$ is a constant, while \hbar and k_B denote the reduced Planck and Boltzmann constants, respectively. Atoms can be regarded as quantum-mechanical wave packets of the order of their thermal de Broglie wavelength $\lambda_T = \sqrt{2\pi\hbar^2 / (mk_B T)}$. The condition for the condensation $T < T_c$ can be reformulated as $l < \lambda_T / \zeta^{-1/3}$, where l is the average distance between pairs of bosons, and it occurs when the temperature, hence the momentum of the bosons decreases such that their de Broglie wavelengths overlap. The thermodynamic limit is only approximately realized, the finite size giving corrections to the critical temperature [45], [46], [47], [48]. A dilute, non-ideal Bose gas also displays BEC, however the condensate fraction is smaller than unity at zero temperature and the critical temperature is also modified [49], [50], [51], [52]. Experimentally, BEC (which could be formed by bosonic atoms, but also form fermionic Cooper pairs) has been realized first in ^{87}Rb [53], [54], [55], then in ^{23}Na [56], [57], and in ^7Li [58].

In a dilute gas, only two-particle interactions dominate. The repulsive, two-body interatomic potential is approximated as $V_{self} = \lambda\delta(\mathbf{r} - \mathbf{r}')$, with a self-coupling constant $\lambda = 4\pi\hbar^2 a/m$, where a is the scattering length. Then in the mean-field approximation (neglecting the contribution of the excited states) the BEC is described by the Gross-Pitaevskii equation [31], [32], [33]:

$$i\hbar\frac{\partial}{\partial t}\psi(\mathbf{r}, t) = \left[-\frac{\hbar^2}{2m}\Delta + V_{selfgrav}(\mathbf{r}) + \lambda\rho(\mathbf{r}, t) \right] \psi(\mathbf{r}, t), \quad (1)$$

where $\psi(\mathbf{r}, t)$ is the wave function of the condensate and Δ is the 3-dimensional Laplacian. The probability density $\rho(\mathbf{r}, t) = |\psi(\mathbf{r}, t)|^2$ is normalized to

$$n_0(t) = \int d\mathbf{r}\rho(\mathbf{r}, t), \quad (2)$$

where $n_0(t)$ is the number of particles and $\rho(\mathbf{r}, t)$ the number density of the condensate. The potential $V_{selfgrav}(\mathbf{r})/m$ is the Newtonian gravitational potential created by the condensate.

Stationary solutions of the Gross-Pitaevskii equation can be found in a simple way by using the Madelung representation of complex wave-functions [59], [60], then deriving the Madelung hydrodynamic equations [59]. Madelung's equations can be interpreted as the continuity and Euler equations of fluid mechanics, with quantum corrections included. However, the quantum correction potential in the generalized Euler equation contributes significantly only close to the boundary of the system [61]. In the Thomas-Fermi approximation the quantum correction potential is neglected compared to the self-interaction term. This approximation becomes increasingly accurate with an increasing number of particles [62].

Assuming a spherically symmetric distribution of the condensate the following solution was found [61], [10]:

$$\rho_{BEC}(r) = \rho_{BEC}^{(c)} \frac{\sin kr}{kr}, \quad (3)$$

where $\rho_{BEC} = m\rho(r)$ and

$$k = \sqrt{\frac{Gm^3}{\hbar^2 a}}. \quad (4)$$

The central density $\rho_{BEC}^{(c)} \equiv \rho_{BEC}(0)$ is determined from the normalization condition (2) as

$$\rho_{BEC}^{(c)} = \frac{n_0 m k^3}{4\pi^2} . \quad (5)$$

The Thomas-Fermi approximation holds valid for $n_0 \gg 1/ka$ [61].

The size of the BEC galactic DM halo is defined by $\rho(R_{BEC}) = 0$, giving $k = \pi/R_{BEC}$, i.e.

$$R_{BEC} = \pi \sqrt{\frac{\hbar^2 a}{Gm^3}} . \quad (6)$$

The mass profile of the BEC halo is then given as

$$\begin{aligned} m_{BEC}(r) &= 4\pi \int_0^r \rho_{BEC}(r) r^2 dr \\ &= \frac{4\pi \rho_{BEC}^{(c)}}{k^2} r \left(\frac{\sin kr}{kr} - \cos kr \right) . \end{aligned} \quad (7)$$

The contribution of the BEC halo to the velocity profile of the particles moving on circular orbit under Newtonian gravitational force becomes [10]

$$v^2(r) = \frac{4\pi G \rho_{BEC}^{(c)}}{k^2} \left(\frac{\sin kr}{kr} - \cos kr \right) , \quad (8)$$

which has to be added to the respective baryonic contribution.

3. Confronting the model with rotation curve data

In order to test the validity of our model, we confront the rotation curve data of a sample of 6 HSB, 6 LSB and 7 dwarf galaxies, with both the NFW DM and the BEC density profiles. For reasons to become obvious during our analysis, we split both the HSB and LSB data sets into two groups (type I. and II.), based on the shapes of the curves. In the first group the rotational velocities increase over the whole observed range, while in the second set the rotation curves exhibit long flat regions.

The commonly used NFW model has the mass density profile

$$\rho_{NFW}(r) = \frac{\rho_s}{(r/r_s)(1+r/r_s)^2} , \quad (9)$$

where ρ_s and r_s are a characteristic density and distance scale, to be determined from the fit.

The mass within a sphere with radius $r = yr_s$ is then given as

$$m_{NFW}(r) = 4\pi \rho_s r_s^3 \left[\ln(1+y) - \frac{y}{1+y} \right] \quad (10)$$

where y is a positive dimensionless radial coordinate.

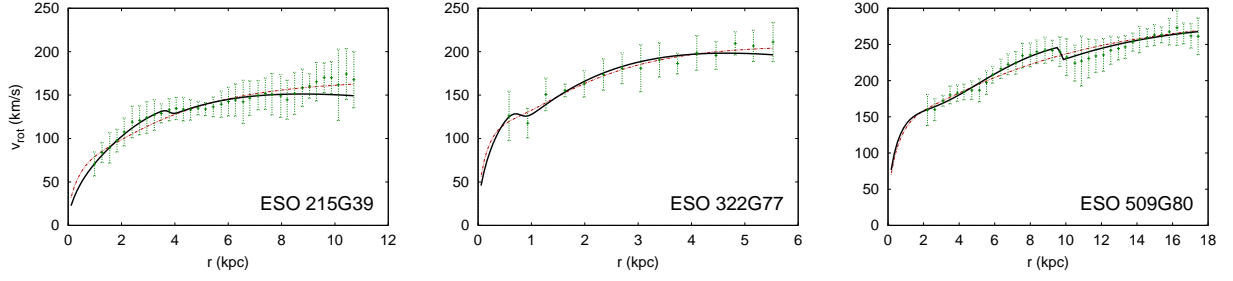


Figure 1. Best fit curves for the HSB I. galaxy sample where the solid black lines hold for the baryonic matter + BEC model, while the dashed red lines refer to the baryonic matter + NFW model.

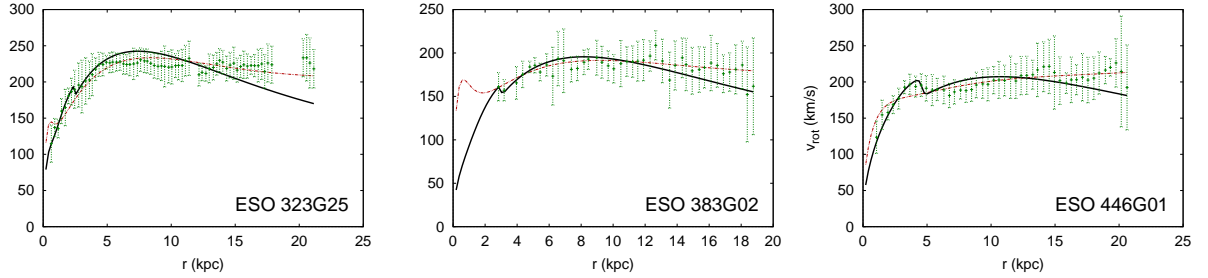


Figure 2. Best fit curves for the HSB II. galaxy sample. The solid black lines hold for the baryonic matter + BEC model, while the dashed red lines for the baryonic matter + NFW model. The BEC model does not describe well the extended flat regions.

Galaxy	D	$I_{0,b}$	n	r_0	r_b	$I_{0,d}^{HSB}$	h^{HSB}
	Mpc	mJy/arcsec ²		kpc	kpc	mJy/arcsec ²	kpc
ESO215G39	61.29	0.1171	0.6609	0.78	2.58	0.0339	4.11
ESO322G77	38.19	0.1949	0.7552	0.33	1.37	0.0744	2.20
ESO509G80	92.86	0.2090	0.7621	1.10	4.69	0.0176	11.03
ESO323G25	59.76	0.1113	0.4626	0.43	0.99	0.0825	3.47
ESO383G02	85.40	0.6479	0.7408	0.42	1.94	0.5118	3.82
ESO446G01	98.34	0.2093	0.8427	1.28	6.33	0.0357	5.25

Table 1. The distances (D) and the photometric parameters of the 9 HSB galaxy sample. Bulge parameters: the central surface brightness ($I_{0,b}$), the shape parameter (n), the characteristic radius (r_0) and radius of the bulge (r_b). Disk parameters: central surface brightness ($I_{0,d}^{HSB}$) and length scale (h^{HSB}) of the disk.

3.1. HSB galaxies

In this subsection we will follow the method described in [15]. In a HSB galaxy we decompose the baryonic component into a thin stellar disk and a spherically symmetric bulge. We assume that the mass distribution of bulge component follows the de-projected luminosity distribution with a factor known as the mass-to-light ratio. We estimate the bulge parameters from a Sérsic $r^{1/n}$ bulge model, fitted to the optical I-band galaxy light profiles.

The surface brightness profile of the spheroidal bulge component of each galaxy is described by a generalized Sérsic function [63]

$$I_b(r) = I_{0,b} \exp \left[- \left(\frac{r}{r_0} \right)^{1/n} \right], \quad (11)$$

where $I_{0,b}$ is the central surface brightness of the bulge, r_0 is its characteristic radius and n is the shape parameter of the magnitude-radius curve.

The respective mass over luminosity is the mass-to-light ratio - for the Sun $\gamma_{\odot} = 5133 \text{ kg W}^{-1}$. The mass-to-light ratio of the bulge σ will be given in units of γ_{\odot} (solar units). We will also give the mass in units of the solar mass $M_{\odot} = 1.98892 \times 10^{30} \text{ kg}$. We assume that the radial distribution of visible mass is given by the radial distribution of light obtained from the bulge-disk decomposition. Thus the mass of the bulge within the projected radius r is proportional to the surface brightness encompassed by this radius:

$$m_b(r) = \sigma \frac{\mathcal{N}(D)}{F_{\odot}} 2\pi \int_0^r I_b(r) r dr,$$

where $F_{\odot}(D)$ is the apparent flux density of the Sun at a distance D Mpc, $F_{\odot}(D) = 2.635 \times 10^{6-0.4f_{\odot}} \text{ mJy}$, with $f_{\odot} = 4.08 + 5 \lg(D/1 \text{ Mpc}) + 25 \text{ mag}$, and

$$\mathcal{N}(D) = 4.4684 \times 10^{-35} D^{-2} \text{ m}^{-2} \text{ arcsec}^2. \quad (12)$$

Therefore the contribution of the bulge to the rotational velocity is

$$v_b^2(r) = \frac{G m_b(r)}{r}, \quad (13)$$

where G is the gravitational constant.

In a spiral galaxy, the radial surface brightness profile of the disk, decreases exponentially with the radius [64]

$$I_d(r) = I_{0,d}^{HSB} \exp \left(- \frac{r}{h^{HSB}} \right), \quad (14)$$

where $I_{0,d}^{HSB}$ is the disk central surface brightness and h^{HSB} is a characteristic disk length scale. The contribution of the disk to the circular velocity is ([64])

$$v_d^2(x) = \frac{G M_D^{HSB}}{2 h^{HSB}} x^2 (I_0 K_0 - I_1 K_1), \quad (15)$$

where $x = r/h^{HSB}$ and I_n and K_n are the modified Bessel functions evaluated at $x/2$, while M_D^{HSB} is the total mass of the disk.

Therefore the rotational velocity in a HSB galaxy, adds up as

$$v_{ig}^2(x) = v_b^2(x) + v_d^2(x) + v_{DM}^2(x). \quad (16)$$

We confront the BEC+baryonic model with (HI and H_{α}) rotation curve data of 6 well-tested galaxies already employed in [15] for testing a brane-world model.

Galaxy	$\sigma(\text{BEC})$	$M_D^{\text{HSB}}(\text{BEC})$	R_{BEC}	$\rho_{\text{BEC}}^{(c)}$	$\chi_{\text{min}}^2(\text{BEC})$	$\sigma(\text{NFW})$	$M_D^{\text{HSB}}(\text{NFW})$	r_s	ρ_s	$\chi_{\text{min}}^2(\text{NFW})$	1σ
	\odot	$10^{10} M_\odot$	kpc	10^{-24}kg/m^3		\odot	$10^{10} M_\odot$	kpc	10^{-24}kg/m^3		
ESO215G39	0.3	5.61	3.8	2.0	23.07	0.6	3.84	187	14.7	22.22	34.18
ESO322G77	1.6	5.1	0.8	89.0	9.15	2.5	3.79	709	8	7.69	11.53
ESO509G80	1.4	48.74	9.7	1.2	12.52	0.9	11	22	800	33.48	36.3
ESO323G25	2.5	12.18	2.5	11.8	222.74	6	9.43	436	6	80.55	66.74
ESO383G02	0.13	8.77	3.0	5.7	48.83	1.7	6.32	459	4.2	23.3	47.9
ESO446G01	0.6	12.77	4.6	5.9	86.02	1.4	6.7	786	4.1	43.37	44.74

Table 2. The best fit parameters and the minimum values (χ_{min}^2) of the χ^2 statistics for the HSB I and II galaxies (the first and last three galaxies, respectively). Columns 2-5 give the BEC model parameters (radius R_{BEC} and central density $\rho_{\text{BEC}}^{(c)}$ of the BEC halo) and the corresponding baryonic parameters (mass-to-light ratio $\sigma(\text{BEC})$ of the bulge and total mass of the disk $M_D^{\text{HSB}}(\text{BEC})$). Columns 7-10 give the NFW model parameters (scale radius r_s and characteristic density ρ_s of the halo) and the corresponding baryonic parameters (mass-to-light ratio $\sigma(\text{NFW})$ of the bulge and total mass of the disk $M_D^{\text{HSB}}(\text{NFW})$). The 1σ confidence levels are shown in the last column (these are the same for both models). For HSB I galaxies the two models give similar χ_{min}^2 values (within 1σ confidence level), however in case of HSB II galaxies with extended flat regions, the NFW model fits better the rotation curves. The χ_{min}^2 values in the case of BEC model are outside the 1σ confidence level for HSB II galaxies.

These were extracted from a larger sample given in [65] by requiring i) sufficient and accurate data for each galaxy and ii) spherical structure of the bulge (no rings and bars). For comparison, the NFW+baryonic model is also tested on the same sample and the respective rotation curves are plotted for both models on Figs. 1 and 2. The small humps on both figures are due to the baryonic component. For the investigated galaxies we have derived the best fitting values of the baryonic model parameters $I_{0,b}$, n , r_0 , r_b , $I_{0,d}^{\text{HSB}}$, h^{HSB} from the available photometric data. The BEC and NFW parameters, respectively were calculated (together with the corresponding baryonic parameters) by fitting these models to the rotation curve data. These are collected in Tables 1 and 2.

Both the BEC and NFW DM models give comparable χ_{min}^2 values (within 1σ confidence level) for HSB I galaxies. In case of galaxies with extended flat regions (HSB II), the NFW DM model fits better the rotation curves, nevertheless BEC model give rotational curves which fall outside the 1σ confidence level.

3.2. LSB galaxies

LSB galaxies are characterized by a central surface brightness at least one magnitude fainter than the night sky. They form the most unevolved class of galaxies [66]. LSB galaxies were found to be metal poor, indicating their low star formation rates as compared to their HSB counterparts [67]. They exhibit a wide spread of colours ranging from red to blue [68] and are characterized by large variety of properties and morphologies. Although the most commonly observed LSB galaxies are dwarfs, a significant fraction of LSB galaxies are large spirals [69].

Our model LSB galaxy consists of a thin stellar+gas disk and a CDM component in a form of BEC. The disk component is the same as for the HSB galaxies, the surface brightness profile being [64]

$$I_d(r) = I_{0,d}^{\text{LSB}} \exp\left(-\frac{r}{h^{\text{LSB}}}\right),$$

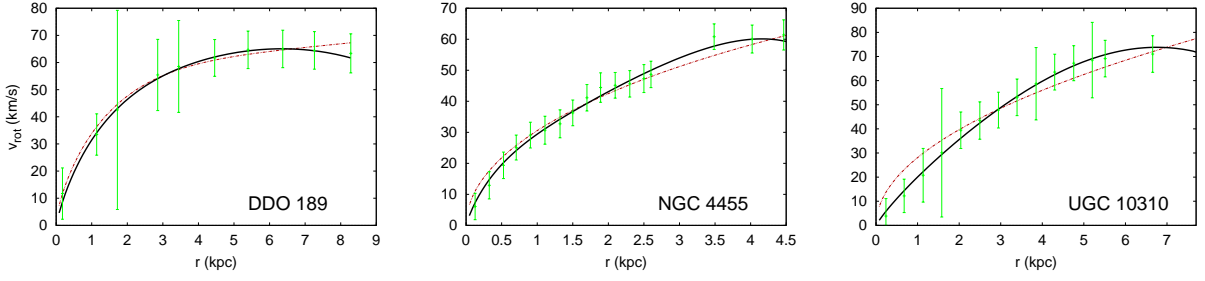


Figure 3. Best fit curves for the LSB I. galaxy sample. The solid black lines hold in the baryonic matter + BEC model, while the dashed red lines in the baryonic matter + NFW model.

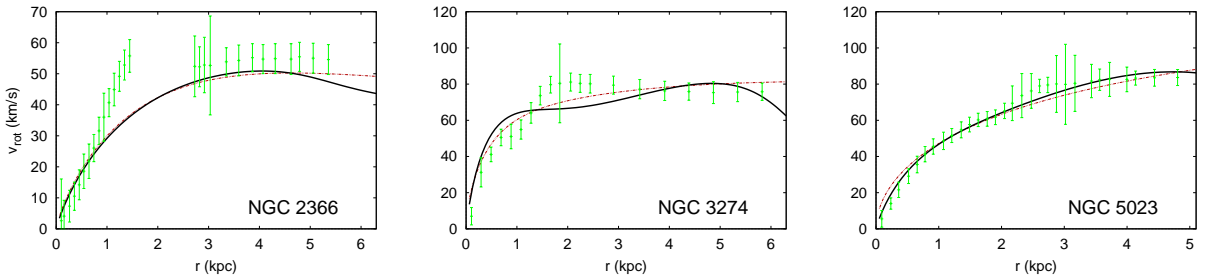


Figure 4. Best fit curves for the LSB II. galaxy sample. The solid black lines refer to the baryonic matter + BEC model, while the dashed red lines to the baryonic matter + NFW model. As for HSB galaxies, the BEC model fails to explain the extended flat regions of the rotation curves.

where $I_{0,d}^{LSB}$ is the central surface brightness and h^{LSB} the disk length scale. We can calculate the disk contribution to the circular velocity as

$$v_d^2(r) = \frac{GM_D^{LSB}}{2h^{LSB}} q^2 (I_0 K_0 - I_1 K_1), \quad (17)$$

where $q = r/h^{LSB}$ and M_D^{LSB} is the total mass of the disk while the modified Bessel functions I_n and K_n are evaluated at $q/2$.

Therefore for a generic projected radius r , the rotational velocity in this combined model is written as

$$v_{ig}^2(r) = v_d^2(r) + v_{DM}^2.$$

A preliminary check confirmed that the BEC+baryonic model represents a better fit than the purely BEC model.

We confronted the BEC model with 6 LSB galaxies taken from a larger sample [70]. The data for these high quality rotation curves are based on both HI and $H\alpha$ measurements. From a χ^2 -test the parameters in both the BEC+baryonic and NFW+baryonic models were identified, these are shown in Table 3. The best fit rotation curves are represented on Figs. 3 and 4.

Galaxy	D	h^{LSB}	$M_D^{LSB}(BEC)$	$\rho_{BEC}^{(c)}$	R_{BEC}	$\chi_{\min}^2(BEC)$	$M_D^{LSB}(NFW)$	ρ_s	r_s	$\chi_{\min}^2(NFW)$	1σ
	Mpc	kpc	$10^9 M_\odot$	$10^{-21} kg/m^3$	kpc		$10^9 M_\odot$	$10^{-23} kg/m^3$	kpc		
DDO 189	12.6	1.9	2.71	0.38	8.3	0.519	2.16	16	70	1.09	7.03
NGC 4455	6.8	0.7	0.231	1.44	5.5	9.29	0	62	39	30.37	18.11
UGC 10310	15.6	1.9	0.443	0.98	7.8	2.66	0	3	660	28.78	13.74
NGC 2366	3.4	1.5	2.43	0.22	5.3	110.73	2.5	0.2	1000	116.93	26.72
NGC 5023	4.8	0.8	0.894	2.45	5.6	53.2	0.0449	457	13	143.08	32.05
NGC 3274	6.7	0.5	1.1	1.69	6.4	269.8	0.252	2373	4	148.44	20.27

Table 3. The best fit BEC and NFW parameters of the LSB I and II type galaxies (the first and last three galaxies, respectively). For LSB I galaxies the BEC DM model gives significantly better fitting velocity curves (within 1σ confidence level) than the NFW model. However the velocity curves are outside the 1σ confidence level for LSB II galaxies.

For LSB I galaxies the BEC DM model gives significantly better fitting velocity curves (all within the 1σ confidence level) compared to the NFW model (which in two cases out of the three gives fits falling outside 1σ). For LSB II galaxies the quality of the fits is comparable, but in both models they are beyond the 1σ confidence level.

3.3. Dwarf galaxies

About 85% of the known galaxies in the Local Volume [71] are dwarf galaxies. They are defined by an absolute magnitude fainter than $M_B \sim -16 mag$, on the other hand they are more extended than globular clusters [72].

The formation history of dwarf galaxies is not well-understood. They formed at the centres of subhalos orbiting within the halos of giant galaxies. Five main classes are distinguished based on their optical appearance: dwarf ellipticals, dwarf irregulars, dwarf spheroidals, blue compact dwarfs, and dwarf spirals. The representants in the last type can be regarded as the very small ends of spirals [73].

All dwarf galaxies have central velocity dispersions in the range $6 \div 25$ km/s [74]. In a typical dwarf galaxy, assuming dynamical equilibrium, the mass derived from the observed velocity dispersions is much larger than the observed total visible mass. This implies that the mass-to-light ratio is very high compared to other types of galaxies, hence they can play an important role in the study of DM distribution on small scales. Dwarf galaxies are ideal objects to prove or falsify various alternative gravity theories [75].

In order to test the BEC model, we have selected a sample of 7 dwarf galaxies for which high resolution rotation curve data is available. We fitted both the BEC+baryonic and the NFW+baryonic models, respectively, with similar baryonic components as for the LSB galaxies. As the length scales of the stellar disks are not available for this sample, they were calculated by χ^2 minimization, too.

A preliminary check showed that the addition of the BEC dark matter halo to the baryonic model improved (giving lower χ_{\min}^2 values) on the fit in all cases. By contrast, the NFW model was unable to improve on the purely baryonic fit in four out of seven cases. We note that since the data does not contain the error margins, the χ_{\min}^2 values are relatively high (beyond the 1σ confidence level in most cases). The best fit BEC and NFW parameters are shown in Table 4 and the corresponding rotation curves are represented on Fig. 5. The inclusion of the BEC DM model gives significantly (in some cases one order of magnitude in the value of χ^2) better fits compared to the case of NFW model. This is due to the cusp avoidance in the central density profile of the

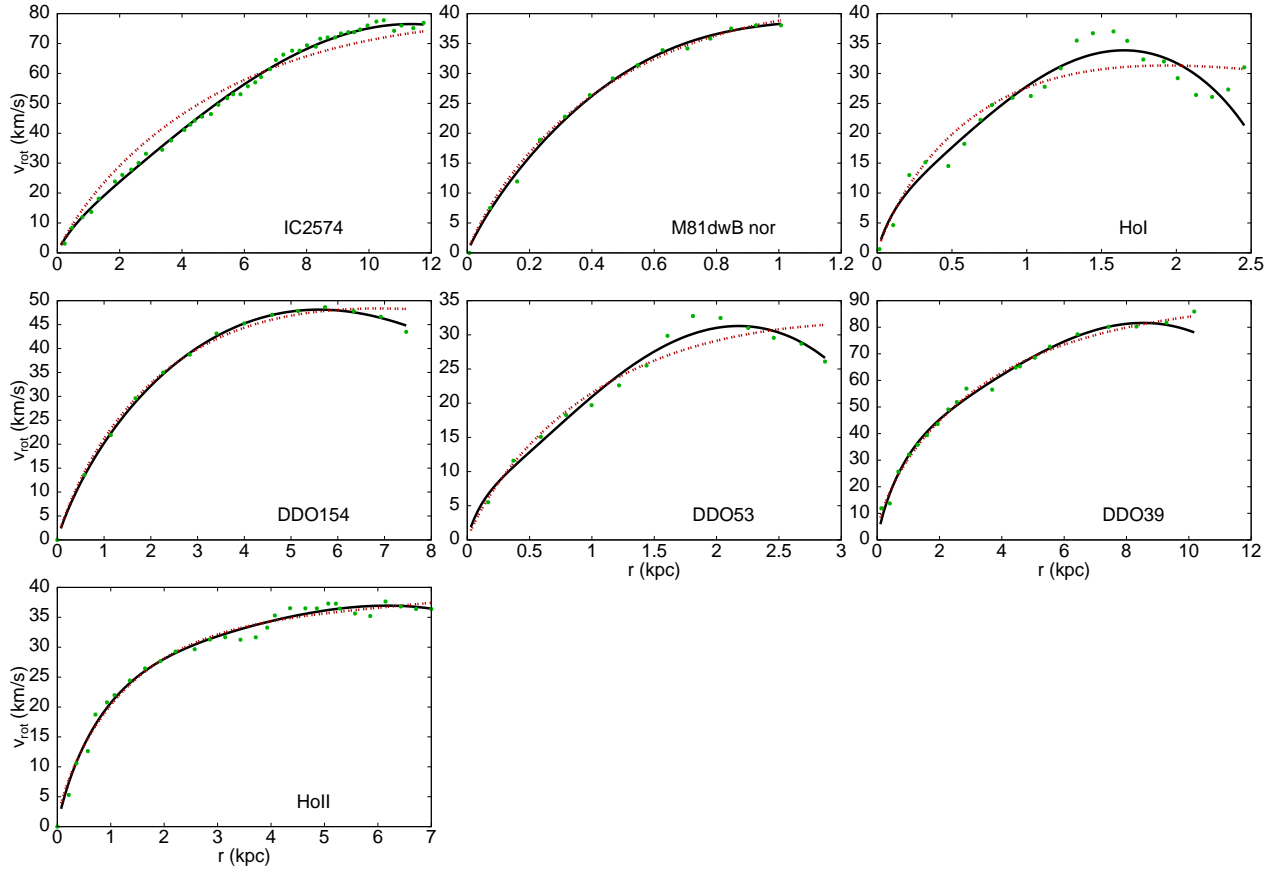


Figure 5. The best fit curves for the dwarf galaxy sample. The BEC+baryonic model (solid black curves) gives a better fit in all cases then the NFW+baryonic model (dashed red lines). In both cases the fit was performed with the same baryonic model.

Galaxy	$h^{dwarf}(BEC)$ kpc	$M_D^{dwarf}(BEC)$ $10^9 M_\odot$	$\rho_{BEC}^{(c)}$ 10^{-24}kg/m^3	R_{BEC} kpc	$\chi_{\min}^2(BEC)$	$h^{dwarf}(NFW)$ kpc	$M_D^{dwarf}(NFW)$ $10^9 M_\odot$	ρ_s 10^{-24}kg/m^3	r_s kpc	$\chi_{\min}^2(NFW)$	1σ
IC 2574	1.2	0.1122	0.4	13	68.47	7.9	28.44	0	0	714.73	44.74
HoI	0.2	0.0107	3.6	1.9	95.26	0.9	0.533	0	0	241.30	20.27
HoII	1.2	0.4431	0.2	7.69	33.33	1.7	0.642	4	92	43.86	26.72
DDO 39	1.3	1.1235	0.7	10.01	69.39	4.3	7.21	43	35	69.82	17.02
DDO 53	0.2	0.0061	1.8	2.5	20.05	1.6	0.976	1	24	51.53	10.42
DDO 154	3.1	3.3502	0.2	5.8	1.48	3.2	4.52	0	0	9.40	9.30
M81dwB nor	0.9	1.023	3.7	0.7	6.19	0.7	0.705	0	0	8.4	10.42

Table 4. The best fit BEC+baryonic and NFW+baryonic parameters for the dwarf galaxy sample.

BEC model and the fact that dwarf galaxies do not exhibit extended flat regions in their rotation curves.

4. A combined test of rotational curves and velocity dispersion profiles

In this section we present the results of a complementary analysis of the projected (line of sight) velocity dispersion of 6 Virgo Cluster galaxies. The chosen sample consists of 6 early-type spiral galaxies, the data of which is taken from [76]. The rotational curve data is also available for these galaxies, therefore we are able to perform a combined χ^2 test. For the two independent data sets $\tilde{\chi}^2$ denotes the sum of the two individual χ^2 values.

In a spherically symmetric and isolated setup the Jeans equation for the velocity dispersion $\sigma(r)$ is [77]

$$\frac{\partial(\rho\sigma^2)}{\partial r} + \rho \frac{\partial\Phi}{\partial r} = 0, \quad (18)$$

where r is the radial distance from the galaxy center, ρ is the mass density and Φ is the gravitational potential. In self-gravitating systems ρ and Φ are related by the Poisson equation. For a given density distribution Eq. (18) can be solved for σ^2 , obtaining for the two models investigated here:

$$\sigma_{BEC}^2(r) = \frac{\rho_{BEC}^{(c)} R_{BEC}^3 G \left[1 - \cos\left(\frac{2\pi r}{R_{BEC}}\right) \right]}{\sin\left(\frac{\pi r}{R_{BEC}}\right) r \pi^2}, \quad (19)$$

$$\begin{aligned} \sigma_{NFW}^2(r) = & 2\pi G r h \rho s r \left(-\ln\left(\frac{r}{rs}\right) (rs+r)^2 rs^{-1} \right. \\ & + \ln\left(\frac{rs+r}{rs}\right) \left(3 \ln\left(\frac{rs+r}{rs}\right) \right. \\ & \times (rs+r)^2 rs^{-1} - 8rs - 4r - 2\frac{rs^2}{r} \\ & + \frac{rs^3}{r^2} + \frac{r^2}{rs} \left. \right) + \pi^2 rs + 2\pi^2 r \\ & + \frac{\pi^2 r^2}{rs} - 9rs - \frac{rs^2}{r} - 7r + 6 \text{dilog} \\ & \left. \times \left(\frac{rs+r}{rs} \right) (rs+r)^2 rs^{-1} \right), \end{aligned} \quad (20)$$

where $\text{dilog}(x) = \int_x^0 \frac{\ln(1-x)}{x} dx$ denotes the dilogarithm function. The line of sight (observed) velocity dispersion σ_{LOS}^2 is given by [78]:

$$\sigma_{LOS}^2(R) = \frac{\int_R^\infty r \sigma^2(r) \rho(r) / \sqrt{r^2 - R^2} dr}{\int_R^\infty r \rho(r) / \sqrt{r^2 - R^2} dr}, \quad (21)$$

with R denoting the apparent distance of the star from the galactic centre in the plane perpendicular to the line of sight. For a realistic model we also include the velocity dispersion contribution of the stellar disk [79]

$$\sigma_d(R) = \frac{6.72 G \tau I_{0d}}{\sqrt{2} v_{\max}} R \exp\left(-\frac{R}{h}\right). \quad (22)$$

Here τ is the mass to light ratio, h is the scale length and I_{0d} is the central surface brightness of the stellar disk.

We fit the BEC and NFW models with the observed velocity dispersion and rotation curve data sets simultaneously (each data sets determined from the Doppler

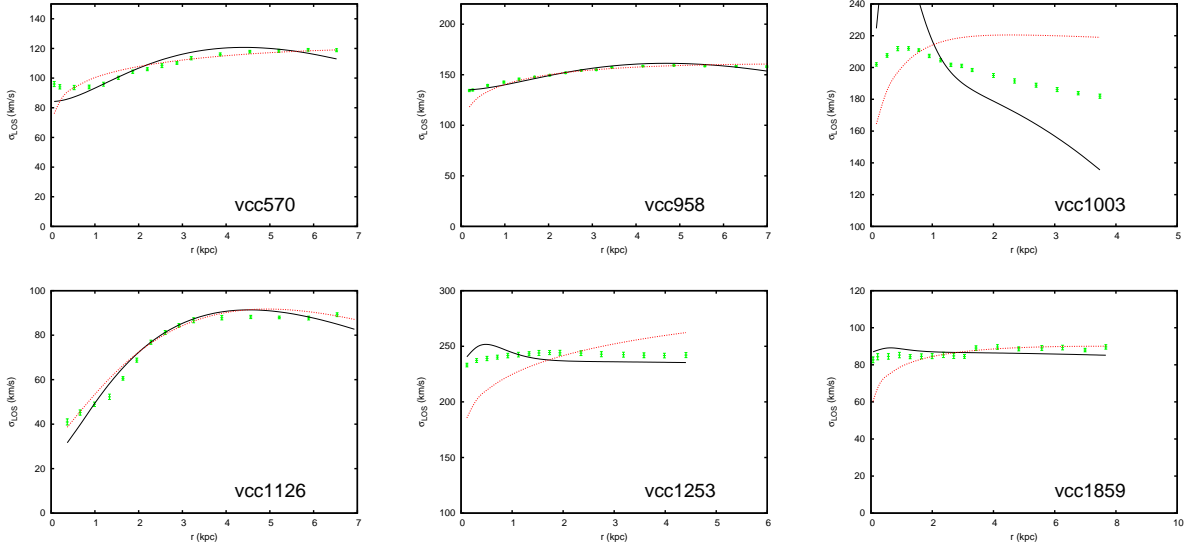


Figure 6. Best fitting line of sight velocity dispersion profiles for the investigated Virgo cluster galaxies. Solid black lines refer to the BEC model, while the dashed red curves to the NFW dark matter model. Both models fit the velocity dispersion data comparably, however the BEC model approximates the data slightly better close to the centres of the galaxies. In case of VCC1003 and VCC1253 the combined tests are completely failed because the best fit parameters are very different for the rotational and velocity dispersion curves as shown in Table 6.

shift), where the subscript DM refers to either of the corresponding dark matter models (i.e. BEC or NFW). The corresponding values of $\tilde{\chi}_{\min}^2$ are given in Table 5. All combined fits are far beyond the 3σ confidence level, hence neither of the models is compatible with both datasets.

For the galaxies VCC1003 and VCC1253 the combined fits were the worst, due to the fact that the best fit parameters for the rotational curve and velocity dispersion data are very different for these galaxies. The parameters of these individual fittings are shown in Table 6. We show the best fit curves for both models resulting from the combined χ^2 -test on Figs. 6 and 7.

5. Discussions and final remarks

We have performed a χ^2 -test of the BEC and NFW DM models, with the rotation curves of a sample of 6 HSB, 6 LSB and 7 dwarf galaxies completed with a combined test of 6 Virgo cluster galaxy rotation curve and velocity dispersion profiles. For improved accuracy we also included realistic baryonic models in every case. For the HSB galaxy sample, both the rotation curve and the surface photometry data were available. Most of the rotation curves were smooth, symmetric and uniform in quality.

For the investigated galaxies, we decomposed in the standard way the circular velocity into its baryonic and DM contributions: $v_{model}^2(r) = v_{baryonic}^2 + v_{DM}^2$. For the BEC model the DM contribution to the velocity is given by Eq. (8). Then the

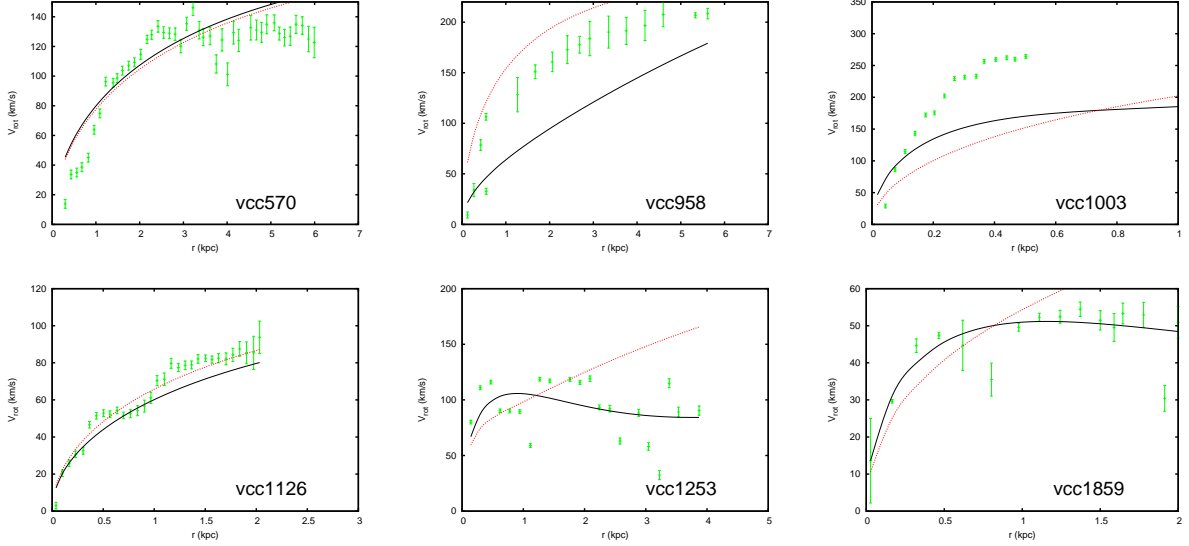


Figure 7. Best fitting rotational velocities for the investigated Virgo cluster galaxies. Solid black lines refer to the BEC model, while the dashed red curves to the NFW DM model. The BEC model gave better fits in two cases (VCC1253 and VCC1859), while for the rest of the galaxies, the predictions of the two models are comparable. In case of VCC1003 and VCC1253 the combined tests are completely failed because the best fit parameters are very different for the rotational and velocity dispersion curves as shown in Table 6.

Galaxy	τI_{0d} kg/m^2	h kpc	R_{BEC} kpc	$\rho_{BEC}^{(c)}$ $10^{-22}kg/m^3$	$\tilde{\chi}_{min}^2(BEC)$	τI_{0d} kg/m^2	h kpc	r_s kpc	ρ_s $10^{-22}kg/m^3$	$\tilde{\chi}_{min}^2(NFW)$	3σ
VCC570	0.61	5.34	10.8	19.6	1365	0.15	10.6	12	11.8	981	88.6
VCC958	0.95	6.33	14.4	28.3	1034	0.42	14	4	186.6	1724	54.7
VCC1003	40.56	0.36	6	344	68578	3.04	1.1	6	180.2	59135	81
VCC1126	0.53	4.58	14	1.12	625	0.45	5	6.2	6	364	72
VCC1253	5.88	0.48	54.1	6.2	2475	4.1	0.21	66	2.8	7654	58.7
VCC1859	0.44	0.62	49.4	1	177	0.07	0.33	15	5	931	53.3

Table 5. The best fit parameters and the minimum values $\tilde{\chi}_{min}^2$ of the combined χ^2 statistics for the 6 Virgo cluster galaxies. Here τ is the mass to light ratio, h is the scale length and I_{0d} is the central surface brightness of the stellar disk. The remaining ones are defined in Table 2.

rotation curves are χ^2 best-fitted with the baryonic parameters and the parameters of the two DM halo models (BEC and NFW).

The analysis of the *HSB I galaxies* showed a remarkably good agreement for both DM models with observations. The quality of the fits of the BEC and NFW models with the rotation curve data was comparable. However the rotation curves of the HSB II type galaxies are significantly better described by the NFW model.

It was previously known that for *LSB galaxies and without including the baryonic sector*, the BEC model gave a better fit than the NFW model [42]. We additionally found that including the baryonic component improves on the fit of [42]. Our detailed

	Galaxy	τI_{0d} <i>kg/m²</i>	h <i>kpc</i>	R_{BEC} <i>kpc</i>	$\rho_{BEC}^{(c)}$ <i>10⁻²²kg/m³</i>	$\tilde{\chi}_{\min}^2(BEC)$	τI_{0d} <i>kg/m²</i>	h <i>kpc</i>	r_s <i>kpc</i>	ρ_s <i>10⁻²²kg/m³</i>	$\tilde{\chi}_{\min}^2(NFW)$	3σ
rot	VCC1003	56.34	1.18	6.02	204.32	2130	38.02	1.01	3.91	383	2113	60.09
	VCC1253	5.5	0.54	37.77	1.97	2260	5.6	0.49	5.24	4.72	2231	36.21
disp	VCC1003	2.11	0.003	7.03	293.77	476	5.03	1.17	6.23	142.46	3634	28.51
	VCC1253	2	0.2	8.24	311.35	1361	3.9	0.77	34.07	9.75	1427	28.51

Table 6. The best fit parameters and the minimum values $\tilde{\chi}_{\min}^2$ of the χ^2 statistics for the VCC1003 and VCC1253 galaxies. The first two lines show the best fit parameters based on the rotation curves data, while the last two lines related to the pure velocity dispersion data fitting. The parameters are the same as in Table 5

analysis showed a significantly better performance of the BEC model for LSB type I galaxies, while comparable fits for LSB type II galaxies. These latter fits were however outside the 2σ confidence level.

The unsatisfactory large distance behaviour of the BEC model for both the HSB and LSB galaxies of type II originates in the sharp cutoff of the BEC DM distribution and clearly indicates that a modification of the BEC model on large distances would be desirable, also to comply with the very distant behaviour of the universal rotation curves (URCs) [80].

A possible alternative is including vortex lattices into the halo ([81]; [44]), as when a BEC is rotated at a rate exceeding certain critical frequency, quantized vortices can be formed. This vortex lattice in principal can influence the galactic rotation curve and provide a flat velocity profile with oscillatory structure ([82]; [42]). One such suggestion takes into account the effects of the finite DM temperature on the properties of the DM halos. An enhanced BEC model which takes into account excited states as suggested in Refs. ([83]; [84]) could significantly modify the DM halo density profiles, such investigations fall however outside the scope of the present paper.

From the above analysis of HSB and LSB galaxies it is also obvious that (while on large distances the BEC model suffers from problems due to the sharp cutoff) close to the it works overall better than the NFW model. This is also supported by our fit of both the BEC+baryonic and NFW+baryonic DM models with rotation curve data of a sample of 7 dwarf galaxies. Since dwarf galaxies are DM dominated, they provide the strongest test of the compared models. The results are shown in Fig. 5. We also note that the NFW DM improved over the pure baryonic fit in four cases out of seven, while including the BEC component improved over the fit with the baryonic component in all cases.

For all cases we have determined the BEC parameters $\rho_{BEC}^{(c)}$, R_{BEC} , given in Tables 2, 3, 4 and 5. The averages of the radii R_{DM} of the BEC halos for the HSB, LSB and dwarf galaxies are $\langle R_{BEC}^{HSB} \rangle \approx 4.06\text{kpc}$, $\langle R_{DM}^{LSB} \rangle \approx 6.48\text{kpc}$ and $\langle R_{DM}^{dwarf} \rangle \approx 5.94\text{kpc}$, respectively. The values of R_{DM} are consistent within the order of magnitude with the halo radii of 59 other galaxies determined from weak lensing ([85]).

The relation among the mass m of the BEC particle, its coherent scattering length a and the radius of the DM halo R_{DM} can be written as ([10])

$$\begin{aligned}
 m &= \left(\frac{\pi^2 \hbar^2 a}{GR_{BEC}^2} \right)^{1/3} \\
 &\approx 6.73 \times 10^{-2} [a(\text{fm})]^{1/3} [R_{BEC}(\text{kpc})]^{-2/3} \text{ eV}.
 \end{aligned}
 \tag{23}$$

In order to constrain the values of scattering lengths, we chose the lower bound of the mass range for the axion, 10^{-6}eV as the particle mass. This gives the following scattering lengths for the three types of galaxies; $a_{HSB} \approx 5.4 \times 10^{-14}\text{fm}$, $a_{LSB} \approx 1.37 \times 10^{-13}\text{fm}$ and $a_{dwarf} \approx 1.15 \times 10^{-13}\text{fm}$. These values are consistent with the results of [85], which are based on a statistical analysis of 61 DM dominated galaxies. The total energy of the BEC halo is negative with these scattering lengths and particle mass, meaning the halo is stable (see Fig. 3. of [35]).

We intended to shed more light on the applicability of these models for describing DM halos through a fit with the velocity dispersion profiles of 6 Virgo cluster galaxies for which the rotation curve data was also available. A combined χ^2 minimization test, fitting the corresponding rotation curve and velocity dispersion data simultaneously showed however quite deceivingly that the combined χ^2 values fall outside the 3σ confidence level for both models, therefore neither of them seems versatile enough to comply with the combination of both type of measurements.

Acknowledgments

MD, ZK and LÁG were supported by the European Union and the State of Hungary, co-financed by the European Social Fund in the framework of TÁMOP 4.2.4. A/2-11-/1-2012-0001 ‘National Excellence Program’. In the early stages of this work LÁG was supported by the Japan Society for the Promotion of Science.

References

- [1] Ade P A R, Aghanim N, Armitage-Caplan C, et al., *Planck 2013 results. I. Overview of products and scientific results*, 2013 submitted to *A&A* arXiv:1303.5062
- [2] Francis M, *First Planck results: the Universe is still weird and interesting*, 2013 *Arstechnica*
- [3] Jalocha J, Bratek L, Kutschera M and Skindzier P., *Global disk model for galaxies NGC 1365, NGC 6946, NGC 7793, UGC 6446*, 2010 *MNRAS* **406**, 2805-2816
- [4] Milgrom M, *A Modification of the Newtonian dynamics as a possible alternative to the hidden mass hypothesis*, 1983 *ApJ* **270**, 365
- [5] Sanders R H, *Anti-gravity and galaxy rotation curves*, 1984 *A&A* **136**, L21
- [6] Moffat J W and Sokolov I Y, *Galaxy dynamics predictions in the nonsymmetric gravitational theory*, 1996 *Phys. Lett. B* **378**, 59
- [7] Mannheim P D, *Are galactic rotation curves really flat?*, 1997 *ApJ* **479**, 659
- [8] Roberts M D, *Galactic metrics*, 2004 *Gen. Rel. Grav.* **36**, 2423
- [9] Boehmer C G and Harko T, *On Einstein clusters as galactic dark matter halos*, 2007 *MNRAS* **379**
- [10] Boehmer C G, Harko T, *Can dark matter be a Bose-Einstein condensate?*, 2007 *JCAP* **06**, 025
- [11] Bertolami O, Boehmer C G, Harko T and Lobo F S N, *Extra force in $f(R)$ modified theories of gravity*, 2007 *Phys. Rev. D* **75**, 104016
- [12] Boehmer C G, Harko T, Lobo F S N, *Dark matter as a geometric effect in $f(R)$ gravity*, 2008 *Astropart. Phys.* **29**, 386
- [13] Mak M K and Harko T, *Can the galactic rotation curves be explained in brane world models?*, 2004 *Phys. Rev. D* **70**, 024010
- [14] Rahaman F, Kalam M, DeBenedictis A, Usmani A A and Saibal R, *Galactic rotation curves and brane world models*, 2008 *MNRAS* **389**, 27
- [15] Gergely LÁ, Harko T, Dwornik M, Kupi G and Keresztes Z, *Galactic rotation curves in brane world models* 2011 *MNRAS* **415**, 3275
- [16] Stabile A and Capozziello P, 2013 *To appear in Phys. Rev. D* arXiv:1302.1760 [gr-qc]
- [17] Primack J R and Gross M A K, *Current Aspects of Neutrino Physics (Springer, Berlin Heidelberg 2000)*, 2000
- [18] de Vega H J and Sanchez N G, *Warm dark matter in the galaxies: theoretical and observational*

- progresses. *Highlights and conclusions of the chalonge meudon workshop 2011*, 2011 *arXiv:1109.3187*
- [19] Wei H, Chen Z and Liu J, *Cosmological Constraints on Variable Warm Dark Matter*, 2013 *Phys. Lett. B* **720**, 271-276
- [20] Biermann P L and Kusenko A, *Relic keV sterile neutrinos and reionization*, 2006 *Phys.Rev.Lett.* **96**, 091301
- [21] Padmanabhan T, *Cosmological constant: The Weight of the vacuum* , 2003 *Phys. Repts.* **380**, 235
- [22] Peebles P J E and Ratra B, *The Cosmological constant and dark energy*, 2003 *Rev. Mod. Phys.* **75**, 559
- [23] Fowlie A, Kowalska K, Roszkowski L, Sessolo E M and Tsai Y L S, *Dark matter and collider signatures of the MSSM*, 2013 *Phys.Rev. D.* **88**, 055012
- [24] G. Aad et al. (ATLAS Collaboration), *Search for Invisible Decays of a Higgs Boson Produced in Association with a Z Boson in ATLAS*, 2014 *submitted to Phys. Rev. Lett.*
- [25] Volker Springel, Simon D M White, Adrian Jenkins, Carlos S Frenk, Naoki Yoshida, Liang Gao, Julio Navarro, Robert Thacker, Darren Croton, John Helly, John A Peacock, Shaun Cole, Peter Thomas, Hugh Couchman, August Evrard, Joerg Colberg and Frazer Pearce, *Simulating the joint evolution of quasars, galaxies and their large-scale distribution*, 2005 *Nature* **435**, 629
- [26] Navarro J F, Frenk C S and White S D M, *The Structure of cold dark matter halos*, 1996 *ApJ* **462**, 563
- [27] Burkert A, *Aspects of Dark Matter in Astro-and Particle Physics*, 1997
- [28] Klypin A and Prada F, , 2009 *ApJ* **690**, 1488-1496
- [29] Gergely LÁ and Tsujikawa S, *Effective field theory of modified gravity with two scalar fields: dark energy and dark matter*, 2014 *to appear in Phys.Rev.D* arXiv:1402.0553 [hep-th]
- [30] Sin S J, *Late time cosmological phase transition and galactic halo as Bose liquid*, 1994 *Phys. Rev. D* **50**, 3650
- [31] Gross E P, *Nuovo Cimento*, 1961 **20**, 454
- [32] Gross E P, , 1963, *J. Math. Phys.* **4**, 195
- [33] Pitaevskii L P, 1961, *Zh. Eksp. Teor. Fiz.* **40** , 646 [Sov. Phys. JETP **13**, 451 (1961)]
- [34] Harko T, *Cosmological dynamics of dark matter Bose-Einstein Condensation*, 2011 *Phys.Rev.D* **83**, 123515
- [35] Souza J C C and Pires M O C, *Discussion on the energy content of the galactic dark matter Bose-Einstein condensate halo in the Thomas-Fermi approximation*, 2014 *JCAP* **03**, 010
- [36] Harko T, *Gravitational collapse of Bose-Einstein condensate dark matter halos*, 2014, [arXiv:1403.3358]
- [37] Lee J W, Lim S and Choi D, *BEC dark matter can explain collisions of galaxy clusters*, 2008 [arXiv:0805.3827v1]
- [38] Rodriguez-Montoya I, Magana J, Matos T and Perez-Lorezana A, *Ultra light bosonic dark matter and cosmic microwave background*, 2010 *ApJ* **721**, 1509
- [39] Velten H and Wamba E, *Power spectrum for the Bose-Einstein condensate dark matter*, 2012 *Phys.Lett. B* **709** 1-5
- [40] Boyanovsky D, de Vega H J and Sanchez N, *Constraints on dark matter particles from theory, galaxy observations and N-body simulations*, 2008 *Phys. Rev. D* **77**, 043518
- [41] Gonzalez-Morales A X, Diez-Tejedor A, Urena-Lopez L A and Valenzuela O, *Hints on halo evolution in SFDM models with galaxy observations* 2012 *Phys. Rev. D* **87** 02130
- [42] Robles V H and Matos T, *Flat Central Density Profile and Constant DM Surface Density in Galaxies from Scalar Field Dark Matter*, 2012 *MNRAS* **422**, 282-289
- [43] Dwornik M, Keresztes Z and Gergely LÁ, *Recent Development in Dark Matter Research* 2014 *Nova Science Publishers* p. 195-219
- [44] Pitaevskii L P and Stringari S, *Bose-Einstein Condensation*, 2003 *Oxford University Press Inc.*, New York.
- [45] Grossmann S and Holthaus M, 1995 *textitZeit. f. Naturforsch.* **50a**, 921; *Phys. Lett. A* **208**, 188
- [46] Ketterle W and van Druten N J, *Two-Step Condensation of the Ideal Bose Gas in Highly Anisotropic Traps*, 1996 *Phys. Rev. A* **54**, 656
- [47] Kristen K and Toms D J, *Bose-Einstein condensation of atomic gases in a general harmonic-oscillator confining potential trap*, 1996 *Phys. Rev A* **54**, 4188
- [48] Haugerud H, Haugset T and Ravndal F, *Bose-Einstein condensation in anisotropic harmonic traps* , 1997 *Phys.Lett. A* **225**, 18
- [49] Giorgini S, Pitaevskii L and Stringari S, *Theory of ultracold atomic Fermi gases*, 1996 *Phys. Rev. A* **54**, R4633

- [50] Glaum K, Pelster A, Kleinert H and Pfau T, *Critical Temperature of Weakly Interacting Dipolar Condensates*, 2007 *Phys. Rev. Lett.* **98**, 080407
- [51] Schütte M and Pelster A, *Critical Temperature of a Bose-Einstein Condensate with $1/r$ Interactions*, 2008 Proceedings of the 9th International Conference, 23-28, September, 2007, Dresden, Germany, Eds. Janke W. and Pelster A., World Scientific Publishing Co. Pte. Ltd., 2008. ISBN #9789812837271, pp. 417-420
- [52] Dalfovo F, Giorgini S, Pitaevskii L P and Stringari S, *Theory of Bose-Einstein condensation in trapped gases*, 1999 *Rev. Mod. Phys.* **71**, 463
- [53] Anderson M H, Ensher J R, Matthews M R, Wieman C E and Cornell E A, *Observation of Bose-Einstein Condensation in a Dilute Atomic Vapor*, 1995 *Science* **269**, 198
- [54] Han D J, Wynar R H, Courteille Ph. and Heinzen D J, *Bose-Einstein Condensation of Large Numbers of Atoms in a Magnetic Time-Averaged Orbiting Potential Trap*, 1998 *Phys. Rev. A* **57**, R4114
- [55] Ernst U, Marte A, Schreck F, Schuster J and Rempe G, *Bose-Einstein Condensation in a Pure Ioffe-Pritchard Field Configuration*, 1998 *Europhys. Lett.* **41**, 1
- [56] Davis K B, Mewes M O, Andrews M R, van Druten N J, Durfee D S, Kurn D M and Ketterle W, *Bose-Einstein Condensation in a Pure Ioffe-Pritchard Field Configuration*, 1995 *Phys. Rev. Lett.* **75**, 3969
- [57] Hau L V, Busch B D, Liu C, Dutton Z, Burns M M and Golovchenko J A, *Near Resonant Spatial Images of Confined Bose-Einstein Condensates in the 4-Dee Magnetic Bottle*, 1998 *Phys. Rev. A* **58**, R54
- [58] Bradley C C, Sackett C A, Tollett J J and Hulet R G, *Evidence of Bose-Einstein condensation in an atomic gas with attractive interactions*, 1995 *Phys. Rev. Lett.* **75**, 1687
- [59] Madelung, E., 1926, *Zeitschrift für Physik* **38**, 322
- [60] Sonogo S, *Interpretation of the hydrodynamical formalism of quantum mechanics*, 1991 *Found. Phys.* **21**, 1135
- [61] Wang X Z, *Cold bose stars: Selfgravitating Bose-Einstein condensates*, 2001 *Phys. Rev D* **64**, 124009
- [62] Lieb E H, Seiringer R and Yngvason Y, *A rigorous derivation of the Gross-Pitaevskii energy functional*, 2000 *Phys. Rev. A* **61**, 043602
- [63] Sérsic J L, 1968, *Atlas de Galaxias Australes*, Cordoba, Argentina, Observatorio Astronomico
- [64] Freeman K C, *On the disks of spiral and SO Galaxies*, 1970 *ApJ* **160**, 811
- [65] Palunas P and Williams T B, *Maximum Disk Mass Models for Spiral Galaxies*, 2000 *ApJ* **120**, 2884
- [66] Impey C and Bothun G, *Low Surface Brightness Galaxies*, 1997 *ARA&A* **35**, 267
- [67] McGaugh S S, *Oxygen abundances in low surface brightness disk galaxies*, 1994 *ApJ* **426**, 135
- [68] O'Neil K, Bothun G D, Schombert J, Cornell M E and Impey C D, *A Wide Field CCD Survey for Low Surface Brightness Galaxies.II. Color Distributions, Stellar Populations, and Missing Baryons*, 1997 *ApJ* **144**, 244
- [69] Beijersbergen M, de Blok W J G and van der Hulst J M, *Surface photometry of bulge dominated low surface brightness galaxies*, 1999 *A&A* **351**, 903
- [70] de Blok W J G and Bosma A, *High-resolution rotation curves of low surface brightness galaxies*, 2002 *A&A* **385**, 816
- [71] Karachentsev I D, Karachentseva V E, Huchtmeier W K and Makarov D I, *A Catalog of Neighboring Galaxies*, 2004 *ApJ* **127**, 2031
- [72] Tammann G A, *Dwarf Galaxies in the Past*, in *Dwarf Galaxies*, 1994 *ESO Conference and Workshop Proc No. 49* p. 3
- [73] Matthews L D and Gallagher J S, *B AND V CCD PHOTOMETRY OF SOUTHERN, EXTREME LATE-TYPE SPIRAL GALAXIES*, 1997 *ApJ* **114**, 5
- [74] Mateo M, *Dwarf galaxies of the Local Group*, 1998 *ARA&A* **36**, 435
- [75] Capozziello S, Cardone V F and Troisi A, *Low surface brightness galaxy rotation curves in the low energy limit of Rn gravity: no need for dark matter?*, 2007 *MNRAS* **375**, 1423
- [76] Ouellette N N Q, *The Dynamical Properties of Virgo Cluster Galaxies*, 2012 PhD thesis
- [77] Binney J and Tremaine S, *Galactic dynamics*, 1987 *Princeton University Press, Princeton*
- [78] Moffat J W and Toth V T, *Testing modified gravity with globular cluster velocity dispersions*, 2008 *ApJ* **680**, 1158
- [79] Bottema R, van der Kruit P C and Freeman K C, 1987 *A&A* **178**, 77
- [80] Persic M, Salucci P and Stel F, *The universal rotation curve of spiral galaxies I. The dark matter connection*, 1996 *MNRAS* **281**, 27
- [81] Zinner N T, *Vortex Structures in a Rotating BEC Dark Matter Component*, 2011 [arXiv:1108.4290v1]

- [82] Yu R P and Morgan M J, *Vortices in a rotating dark matter condensate*, 2002 *Class. Quantum Grav.* **19** L157
- [83] Harko T and Madarassy E J M, *Finite temperature effects in Bose-Einstein Condensed dark matter halos*, 2011 [arXiv:1110.2829v1]
- [84] Robles V H and Matos T, *Exact Solution to Finite Temperature SFDM: Natural Cores without Feedback*, 2013 *ApJ* **763**, 19
- [85] Pires M O C and de Souza J C C, *Galactic cold dark matter as a Bose-Einstein condensate of WISPs*, 2012 [arXiv1208.0301]